Universiteit Utrecht

Opleiding Natuur- en Sterrenkunde

An analysis of the binary black hole merger GW150914

Bachelor Thesis

Suzanne Lexmond

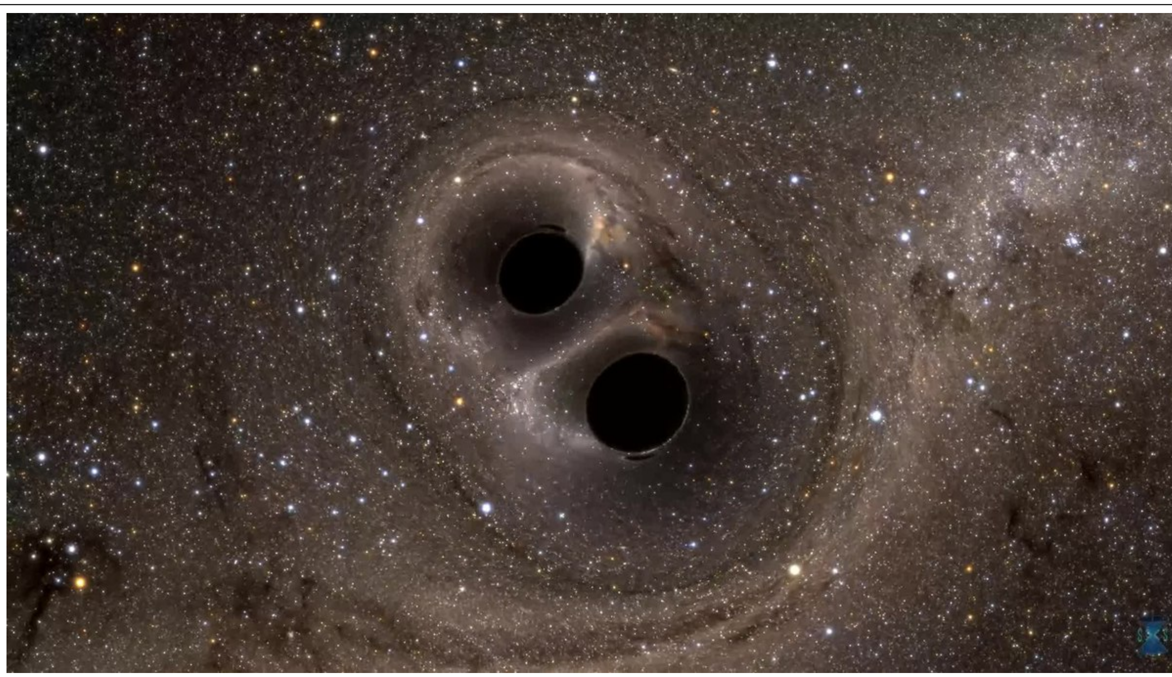

Supervisors:

Prof. Stefan Vandoren
Institute of theoretical physics

Dirk Schuricht
Institute of theoretical physics

15/01/2020

Abstract

On September 2015 LIGO observatories detected the very first gravitational wave signal. Since than gravitational waves play a large role of interest in modern day science. This thesis takes a closer look at the first observed gravitatational wave signal, GW150914. It analyses the signal by first extracting the merger from the incoming data strain filled with dominant noise than being compared with a theoretical general relativity template. When the signal is extracted, the data is analyzed with Newtonian mechanics and compared to the publicly published data from LIGO. At last, it is briefly discussed how general relativity plays a large role in black hole mergers, also deriving the Einstein field equations.

The figure on the title page shows the binary black hole merger of GW150914. It is a computer simulated figure clearly showing the distortion of space-time due to the strong gravitational field of the black holes. This simulation is made by the SXS project (1).

Contents

1 Introduction 1

2 Gravitational waves 2
- 2.1 What are gravitational waves? 2
- 2.2 Gravitational waves in the geometry of space-time 3
  - 2.2.1 Flat spacetime 3
  - 2.2.2 Linearized gravitational waves 4
- 2.3 Detecting gravitational waves 5
  - 2.3.1 Laser interferometers 5
  - 2.3.2 Noise cancellation 7
  - 2.3.3 Current gravitational wave detectors 8
  - 2.3.4 The Einstein Telescope 10
  - 2.3.5 LISA 10

3 Binary black hole mergers 12
- 3.1 Black holes 12
- 3.2 Binary black hole mergers 13

4 Data analysis of the GW signal 16

5 Physical aspects of a BBH merger 22
- 5.1 Newtonian mechanics 22
- 5.2 General relativity 25

6 Discussion and conclusion 30

7 Appendix 33

1 Introduction

In 1916, Albert Einstein was the first to predict the existence of gravitational waves. He already knew that the amplitude of these gravitational waves would be extremely small and therefor very hard to detect. Until on 14 september 2015 LIGO observatories did the impossible and discovered the very first gravitational wave signal which they called GW150914. The signal came from a binary black hole merger with masses of 36 $M_{\odot}$ and 29 $M_{\odot}$, 1.4 billion light years away. Since than science has come a very long way in discovering many more signals from different sources of gravitational waves. So far we have only been able to detect gravitational waves from events with extremely high mass and acceleration, like binary black holes, binary neutron stars and neutron star-black hole mergers. Since the discovery in 2015 the field of gravitational waves is strongly making it's way in science. Today there are multiple detectors looking for new discoveries and plans for newer and better detectors are already being made.

With this new gravitational wave data, the theoretical predictions of Einstein and many more can now finally be confirmed. So far Einstein's theory of general relativity seems to be in agreement with the discovered data, but many more observations to come will prove if this indeed is true.

This thesis takes a closer look at the analysis of the GW150914 signal. The incoming signal will be studied using several filtering techniques so the real gravitational wave signal can be extracted. It will be studied for its properties and compared with theoretical expectations of binary black hole mergers. Finally, using Newtonian mechanics, the data is checked and compared with the published data from LIGO. To determine an exact theoretical template of a gravitational wave signal, knowledge of general relativity is demanded. This thesis does not widely look into the field of general relativity but does discuss some main ideas in this area. We show how general relativity is crucial in binary black hole mergers, at last deriving the Einstein field equations.

2 Gravitational waves

2.1 What are gravitational waves?

In 1916 Einstein was the first to predict the existence of gravitational waves. With his theory on general relativity he completely changed the idea of time. He described these gravitational waves as wripples in space-time much like waves moving in water. These gravitational waves would be emitted by massive accelerating bodies, moving with the speed of light.

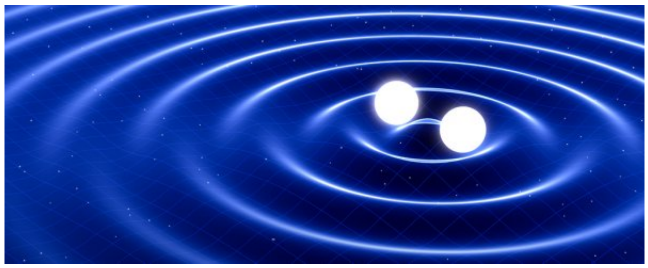

Figure 1: The distortion of gravitational waves in space-time. (2)

Even though Einstein started the great theory it was not until 1974 when Russell Alan Hulse and Joseph Hooton Taylor discovered the first real proof on gravitational waves (3). What they found was a binary pulsar system acting exactly as the theory of general relativity predicted. The decay of the orbital period matched the energy loss and loss of momentum in gravitational radiation. This discovery earned them a Nobel prize. Since than many more discoveries have been made for other pulsar binary systems.

Then on september 14, 2015, the LIGO observatories made the first ever direct detection of two merging black holes nearly 1.4 billion light years away. Finally, proving Einstein's theory of relativity. Since then there have been many observations of gravitational waves from an entire network of detectors, all consistent with the theory of general relativity.

Just like electromagnetic waves there is also a broad spectrum of gravitational waves based on different kind of frequencies. Gravitational waves are known to have much lower frequencies and the wavelengths differ from hundreds of kilometers to the span of the universe. Bigger masses produce lower frequencies. So far earth based interferometers have only been able to detect signals from extremely massive objects up to frequencies of a few kilohertz.

Gravitational waves have a lot in common with the electromagnetic spectrum but differ from them in a couple of ways. Since they are produced by the motion of extremely large masses, spinning at relativistic speeds, their wavelength is in general larger than the objects themselves. They propagate in vacuum, leaving behind wripples in the curvature of space-time. They are considered very weak compared to other know forces and do almost not (considered not) interact with matter. This causes them to barely weaken over long periods of time, making it possible for us to detect gravitational waves from maybe as long ago as the big bang. They contain a lot of useful information about their distances and certain parameters such as mass and spin of the emmiting bodies. However since they are so weak, there is a high form of precision needed to measure these parameters. Therefor it is highly necessary to compare the results with solutions of earlier determined gravitational two-body system using general relativity.

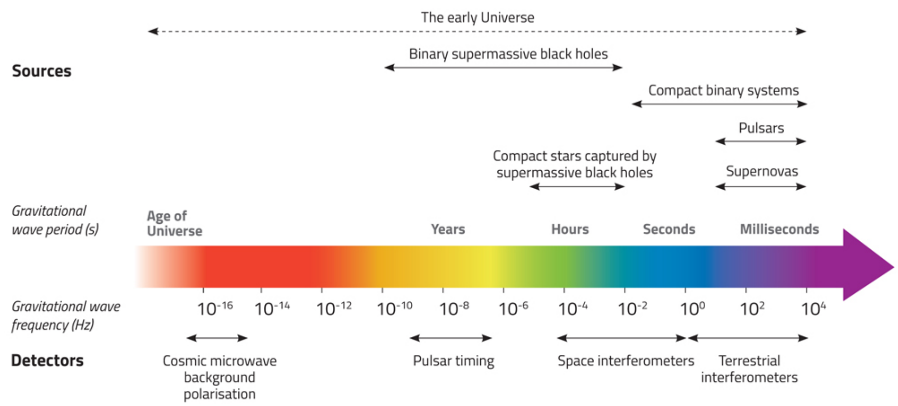

Figure 2: The gravitational wave spectrum of different frequencies. (4)

So far it is only possible to detect relatively high frequencies of large masses like supernovas, compact binary systems and pulsars. This thesis will focus on binary black hole systems.

2.2 Gravitational waves in the geometry of space-time

2.2.1 Flat spacetime

Minkowski space was formed to specify the distance between two points in spacetime. It is a combination of three-dimensional Euclidean space with an added fourth-dimension of time. This is done by using the four Cartesian coordinates (t, x, y, z) and a different set of coordinates (t', x', y', z') for an inertial frame. It is mostly used in Einstein's special relativity. To make the connection between these inertial frames, Minkowski space defines a spacetime interval between two events as the following,

$$ds^2 = -cdt^2 + dx^2 + dy^2 + dz^2 \qquad (1)$$

$$\eta_{\alpha\beta} = \begin{pmatrix} -1 & 0 & 0 & 0 \\ 0 & 1 & 0 & 0 \\ 0 & 0 & 1 & 0 \\ 0 & 0 & 0 & 1 \end{pmatrix} \qquad (2)$$

With the Minkowski metric for flat space defined as $\eta_{\alpha\beta}$.

2.2.2 Linearized gravitational waves

Gravitational waves can be defined by some basic properties; they move at the speed of light, are transverse, have two polarizations, they can be detected by their effect in the motion of test masses, and they carry energy. Since gravitational waves are wripples in space-time, they are often expressed as perturbations from flat space-time. This can be formulated as a metric where gravitational waves are composed of the Minkowski metric $\eta_{\alpha\beta}$, representing flat space-time, adding a perturbation metric $h_{\alpha\beta}$,

$$g_{\alpha\beta} = \eta_{\alpha\beta} + h_{\alpha\beta}, \tag{3}$$

where $\eta_{\alpha\beta}$ can be defined as above and $h_{\alpha\beta}$ can be defined as,

$$\eta_{\alpha\beta} = \begin{pmatrix} 0 & 0 & 0 & 0 \\ 0 & 1 & 0 & 0 \\ 0 & 0 & -1 & 0 \\ 0 & 0 & 0 & 0 \end{pmatrix} f(t-z), \tag{4}$$

where f is a function of $t - z$. Another property mentioned above is that gravitational waves have two independent polarizations. The polarization is a linear combination of a so called cross-polarization $h_\times$ and a plus polarization h_+ that are both transverse to the direction of propagation,

$$h = F_\times h_\times + F_+ h_+, \tag{5}$$

where F and F_+ are called the form factors which depend on the direction and orientation of the source with respect to the detector. The cross- and plus polarization are just as the polarization of electromagnetic waves only are the polarizations of gravitational waves 45° apart instead of 90°. The effects of polarization on test masses is shown in fig.3. (5)

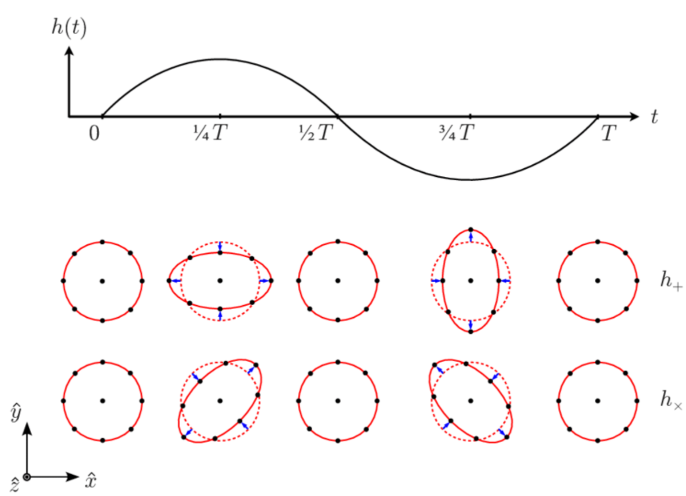

Figure 3: The effects of polarization for $h_\times$ and h_+ on several test masses. (6)

2.3 Detecting gravitational waves

Gravitational waves can travel from billions of light years away. This makes it difficult to observe direct detections. While they travel, the amplitude of the waves decrease which makes even the largest waves only the size of an atom when reaching earth. Currently, it is only possible to detect gravitational waves coming from really large sources. The strongest gravitational waves arise from the most violent events such as large binary systems existing of black holes or neutron stars. While the bodies orbit around each other the distance between them will get smaller because of energy loss caused by the emission of gravitational waves. For the frequency to be high enough to detect the gravitational waves, the bodies need to be massive with a high enough orbiting velocity. To detect the gravitational waves of smaller bodies we will have to wait for better space-based detectors. (7)

2.3.1 Laser interferometers

Since 2015, interferometers have finally made it possible to directly detect gravitational waves. An interferometer merges beams of light to create an interference pattern. This pattern caries information about the time of contact between two or more lightwaves. In 1880 Albert Michelson was the first to invent an interferometer. An Interferometer consists of a laser, a beam splitter, 2 mirrors and a photodetector as presented in fig. 4. The beamsplitter splits the laser in two separate paths, both travelling the same identical pathlength. Both being reflected by a mirror at the end, to come together again at the source. If the path of the two beams would have been identical, the amplitudes would cancel, causing there to be no light left at the photo detector.

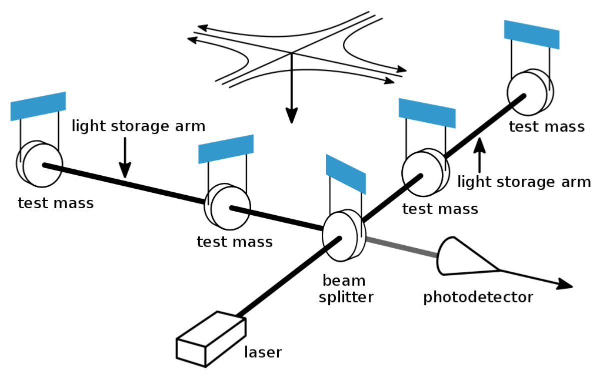

Figure 4: Schematic of a gravitational wave detector. (8)

An interferometer consist of two long arms. When gravitational waves make contact with an interferometer the space around it will stretch while the space in the direction perpendiculair to it will compress. The two arms being in perpendiculair direction of each other will cause one arm to shorten while the other becomes longer resulting in a relative change in pathlength,

$$h = \frac{2\delta L}{L} = 10^{-22}. \tag{6}$$

This difference in pathlength causes the waves to create an interferencepattern that no longer results in two cancelling amplitudes. Since the amplitude of the gravitational waves measured on earth are of such small size, the changes done to the pathlength are very minimal (can be as small as 10^{-19} m) which makes it very hard to detect. This difference in path length can easily be caused by all kinds of noise. This makes them very important for a detector to use the best isolation possible.

For the gravitational wave detectors to pick up a signal of the order of 10^{-22}, the Michelson interferometer has to be adjusted with a few extra modifications;

Power enlargement
If we look at the sensitivity of a single photon with an average wavelength of 10^{-6} m for a detector that has an optical pathlength of 4 km, the relative change in pathlength would be,

$$h \approx \frac{\lambda/2}{L_{optical}} \approx 10^{-10}. \tag{7}$$

To have the right amount of power the relative pathlength needs to be at least 10^{12} bigger. To make the detectors more sensitive, a power is needed of 20 MW, while the detector with currently the largest known power can only generate a power of 18 W. This means other adjustments have to be made.

Mirror cavities
Another way to increase the sensitivity is to increase the relative pathlength. This can be done by circulating the signal in between cavities, build of partially reflecting mirrors. By adding two mirrors on both arms the relative pathlength can be increased equally.

Power recycling
Another way to increase the power is by placing a partially transmitting mirror between the laser and the beamsplitter. This way the power that gets lost by returning to the laser gets summed with new fresh photons, increasing the power.

Signal recycling
By placing another partially reflecting mirror between the beam splitter and the photodetector the signal gets summed coherently with fresh signal to increase the power.

Fig. 5 shows an adjusted version of the Michelson interferometer, applying all the techniques mentioned above, resulting in a gravitational wave detector strong enough to pick up signals of the order of 10^{-22}. This is the basis used by most currently existing interferometers. (9)

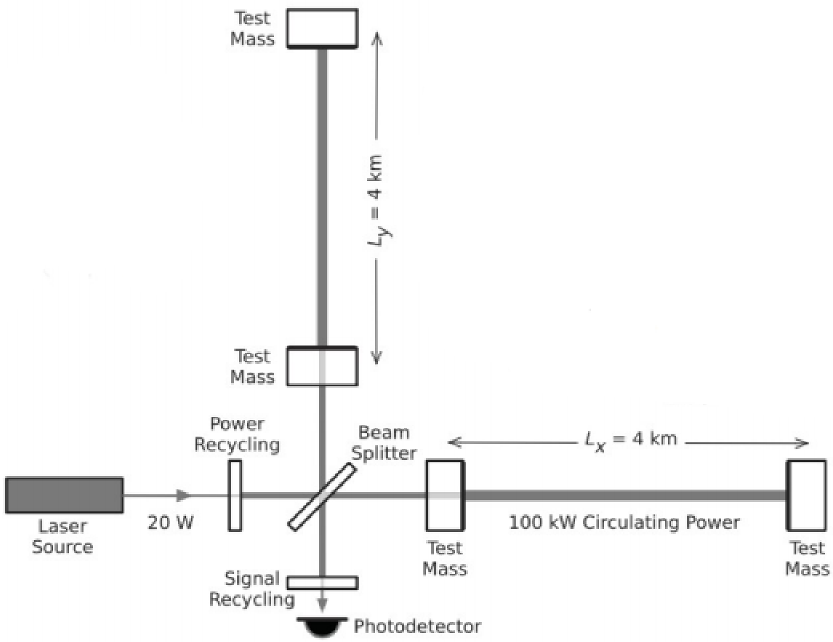

Figure 5: A Michelson interferometer adjusted with extra mirror cavities, power recycling and signal recycling. (9)

2.3.2 Noise cancellation

Since a gravitational wave signal is of such small size, sensitivity of the detector is most important. However the more sensitive the detector becomes, the more noise it detects. There are a lot of different kinds of sources that preduce noise which ask for different approaches of noise cancelling for which some will be discussed;

Shot noise
Shot noise is a form of noise that occurs because of photon counting errors. It is known that some moments there arrive more photons on the photodiode than others which cause these counting errors. These errors are dependent on the photon flux by means of a Poisson distribution. The photon flux depends on the power like,

$$\overline{N} = \frac{P}{h\nu}. \tag{8}$$

This results in a photon counting error of $\Delta P_{shot} = \sqrt{2h\nu P \Delta f}$

Radiation pressure
The photons arriving at the mirrors carry momentum causing a mechanical pressure on the surface of the mirrors. A more powerful signal causes a higher mechanical pressure.

Seismic noise
Vibrations in the earth can also be a source of noise. This can be as a result of several

reasons like tectonic movements, lunar tides, ocean waves or wind. It is also very dependent on the weather causing more noise on heavier days. It is also more convenient to measure on nights since days are often a bigger source of noise. Seismic noise is often partly resolved with multiple pendulum systems, applying a force to the test-mass.

Thermal noise
Thermal noise is caused by random movement of free electrons in conducting materials. It appears in two forms; The first one appears in the wires needed for holding the test-masses, while the second one appears in the mirrors. It limits the sensitivity in the frequency range of 50-500 Hz. Currently, a new method of using cryogenic temperatures for minimizing thermal noise is being discussed.

These are only a few in the huge spectrum of sources that are able to cause noise. Fig.6 shows the sensitivity curve of advanced LIGO for a few different kinds of noise and their amplitudes. It can be noticed that the noise is mostly apparant around the low- and high frequency range. For low frequencies there is a large source of radiation pressure noise, while in the high frequency range the shot noise plays a dominant role.

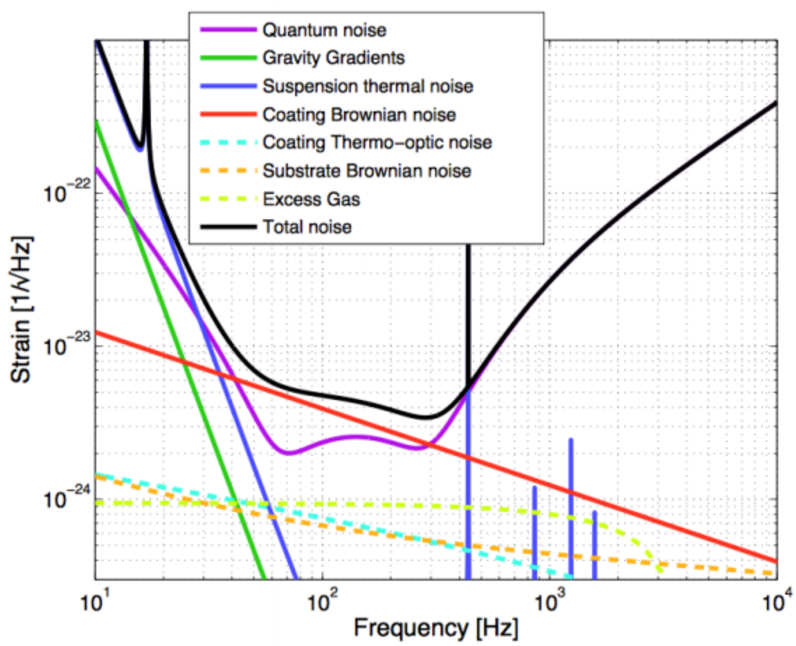

Figure 6: Advanced VIRGO's sensitivity curve for different kinds of noise. (9)

2.3.3 Current gravitational wave detectors

LIGO is currently the world's largest and most sensitive gravitational wave detector (10) . It consist of two interferometers that each have two 4 km long arms. One in Hanford and the other one in Livingston. LIGO consist of two detectors so it can distinguish noise from real gravitational waves when a signal is being measured at both detectors. Especially the LIGO technology used for noise cancellation is most impressive. It uses seismic isolation systems, vacuum systems, the best optics components and a computing infrastructure. The seismic isolation consists of two working mechanisms of active and passive damping. The active demping is made of devices that are able to dampen out the noise by analyzing the frequency and sending out a compromising signal. The passive demping system makes sure all of the mirrors are kept perfectly still by using a quadruppel quad consisting of vibrational damping masses. LIGO possesses one of the largest sustained vacuums in the world. The vacuum makes sure that no molecules present in the air are able to create noise by getting in contact with the system. The vacuum also lowers the changes of dust getting in the way of either the path of the lasers or possibly the mirrors. LIGO also uses the best optical system starting with a 200W laser beam. The mirrors are made of the highest quality available, which is sillica glass. It absorbs just one in 3 million photons for the highest level of reflection to maintain the best resolution.

(a) LIGO, Washington State and Livingston. (10)

(b) VIRGO, Cascina. (11)

Figure 7: Gravitational wave detectors on earth.

VIRGO is the largest gravitational wave detector in Europe and is located in Cascina, Italy (11). It's arms are both 3 km long with an effective optical path of 120 km per arm extended by multiple mirror reflections. VIRGO as well uses only the best techniques for noise cancellation. It uses high power ultrastable lasers, high reflectivity mirrors, seismic isolation and position and alignment control. For the seismic isolation VIRGO uses a 10 m high system of compound pendulums. The vacuum tubes are the second largest high vacuum vessels in the world.

When searching for gravitational wave signals, collaboration between multiple detectors is highly necessary. Because of the great sensitivity a gravitational wave detector requires it is also very easy to mistake a possible signal for noise. By using multiple detectors, the same signal can be verified by appearing at the same time for different detectors. Another requirement is for the detectors to be a great distance apart so the detectors do not mistake the same noise for a real signal. So far the two detectors from LIGO form a collaboration with VIRGO to build a network of three interferometers increasing the reliability of the measurements. An even bigger network of interferometers is already being worked on. Currently, Japan is building a 3 km long interferometer which will be joining the LIGO/VIRGO collaboration when ready. KAGRA will be using cryogenic systems to cool down the optics which will decrease the vibrational noise even further. Besides the 3 current existing interferometers, another detector, the GEO600, lies in Germany with the armlength of 0.6 km also serving as a test object to seek for new optical systems in future detectors.

Another reason for building a network of multiple interferometers is the ability of sky-localization. To localize the emission source, multiple detectors have to focus on the same signal. By analyzing the time delay and loss in amplitude between different detectors we can approximate a certain region from where the signal is supposed to be emitted. Fig.9 shows how LIGO and VIRGO working together on the sky localization map have come to cover just 60 square degrees compared to hundreds without the collaboration of VIRGO. (12)

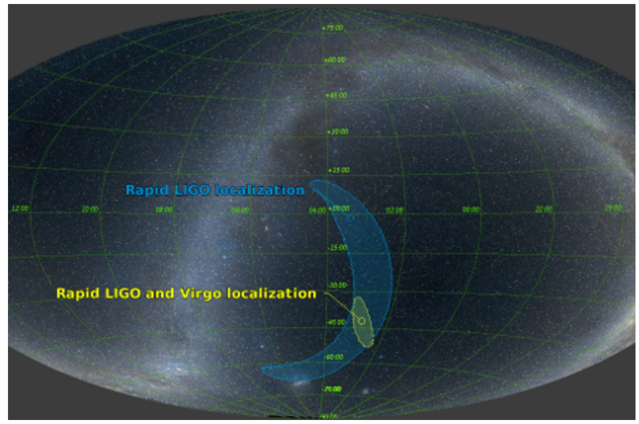

Figure 8: Sky localization of the two LIGO detectors compared to the addition of VIRGO. (13)

2.3.4 The Einstein Telescope

The Einstein telescope (ET) is a project for the newest gravitational wave detector in cooperation of The Netherlands, Belgium and Germany. The ET will be the most sensitive detector yet and will contain three arms in triangular pattern, each consisting of two interferometers for high- and low frequencies. The broad frequencyband will give the opportunity to look into different paths of the universe. The arms are planned to be 10 km long which will make them by far the largest in the world. These features are supposed to make the detector 10 times more sensitive than the best current detectors and are predicted to detect up until a 1000 times more sources of gravitational waves. It is predicted to find new gravitational wave events several times a day compared to several times a year by current detectors. For now, it is still debated if the detector will be located in either Sardinia or the Netherlands. Construction is planned to be in the year of 2025. The ET will be the first third-generation telescope which means that the current telescopes do not have the ability to ever be upgraded on to this level of precision. (14)

2.3.5 LISA

The LISA project is the first idea for a gravitational wave detector in space. LISA is a combined project from the ESA (European space agency) and NASA. A gravitational wave detector in space would give a lot of opportunities which can not be accomplished on earth. The large amount of space makes it possible to provide LISA with three laser interferometers arms of each 2.5 billion km long, shaped in a triangular pattern. This armlength has been chosen to detect signals in the frequency range of 0.1mHz to 100mHz, which would not be possible on earth. This new frequency range will give us an entire new spectrum of gravitational wave sources to explore. This frequency range will make it possible to observe new events like; the observation of black holes and galaxy formations, the merger of massive black holes in galaxies at all possible distances, the merger of massive black holes with other object, binary compact stars and stellar remnants, more distant binaries and possible even sources that are currently unknown. This new frequency range will give us opportunities to explore the structure of the universe even further. LISA will be able to accomplish an exceptional strain resolution of 10^{-20} and a directional precision of one square degree.

The structure of LISA will excist of three free-falling test masses, each protected by a spacecraft to prevent any disturbances of noise. The free-falling test masses will prevent any seismic and gravity-gradient noise which does play a large role in detectors build on earth. Being in space it also has a very stable thermal environment resulting in a minimum of thermal noise. The triangular system of arms will orbit the sun while following earth, keeping a closely constant distant.

The first tests to put LISA in space have already been made. LISA pathfinder was launched on december 2015 and succeeded to put two well functioning free-falling test masses in space with results exceeding the expectations. The planned launch for LISA will be in 2030. (15)

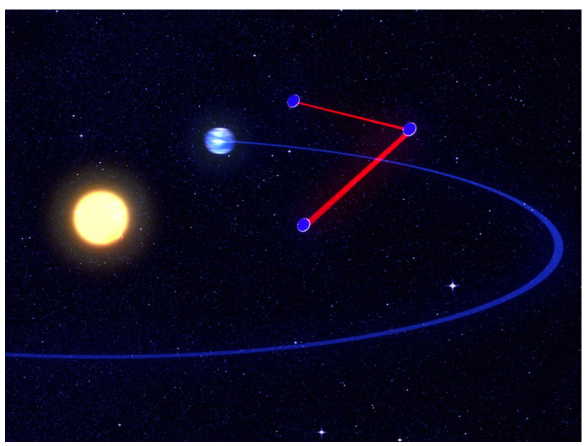

Figure 9: The LISA space project will consist of three 2.4 billion km long arms orbiting in sun with a small distance from earth. The laser-interferometer will be measuring frequencies in a new low frequency range. (16)

3 Binary black hole mergers

3.1 Black holes

Albert Einstein was not only the first to predict gravitational waves but also the first in line to predict the existence of black holes during 1916. Not so long ago this was nothing more than a theorical assumption until last April 2019, when the first photographic proof of a black hole was finally there. An image of this can be seen in fig.10. The first photographic proof came from the Event Horizon Telescope collaboration and was of the supermassive black hole M87* at the center of the Messier 87 galaxy.

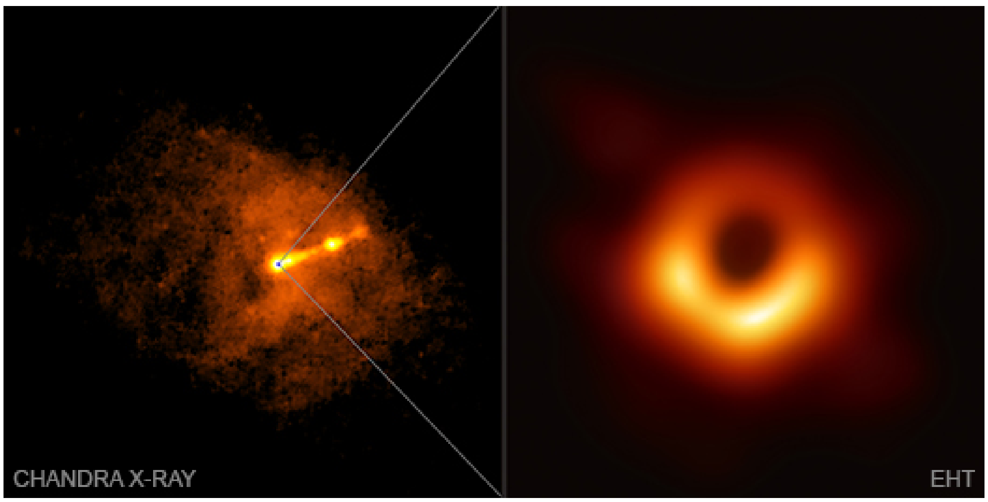

Figure 10: First photografhic proof of a black hole, M87*. The image on the left was taken by NASA's Chandra X-ray observatory. The radio image on the right was taken by the Event horizon telescope. (17)

Black holes can be classified in different groups depending on their mass and origin. After forming, they can always gain mass by accreting dust and gas from nearby galaxies. They are classified in the following groups:

Stellar black holes:
Stellar black holes are formed through stellar evolution of the larger stars. When an evolving star has a mass larger than the Tolman−Oppenheimer−volkoff limit (TOV) the star will eventually evolve into a black hole. At a certain point the nuclear force created by stellar energy sources will exhaust which results in a gravitational collapse of the star. When the star is massive enough, the gravitational forces will become so strong that the evolution results in the creation of a black hole. Depending on the mass of the star before evolution, the mass of the black hole will be smaller or larger. Black holes formed by stellar collapse are relativily small but are known to be extremely dense. Stellar black holes mostly vary from masses between $5M_{\odot}$ to $10M_{\odot}$.

Supermassive black holes:
Most black holes are known to be supermassive black holes. Their masses seem to vary around hundred of thousands of solar masses ($10^5 M_\odot - 10^9 M_\odot$). They are known to lie at least at the center of every galaxy. There are a few theories on how they are formed. They may have been formed by smaller black holes merging together or large gas clouds collapsing into quasi-stars. Another possibility is the collapse of entire stellar clusters. Some think it might be from large clusters of dark matter. Finally, another theory would be a primordial black hole, which are formed in the first moments after the big bang, having a lot of time to absorb more mass.

Intermediate black holes:
Intermediate black holes haven't been known for a very long time. Scientists used to believe that there would only be small or large sized black holes. Since they are too massive to form from stellar collapse of a single star they were not thought to exist. They can be formed by the merger of stellar black holes and other compact bodies threw accreting these masses. They are also though to be primordial black holes. Another way could be as a result of chain reactions during the collision of massive stars in stellar clusters with relatively high densities. Their masses lie within the range of $10^2 M_\odot - 10^5 M_\odot$. (18)

3.2 Binary black hole mergers

To detect gravitational waves that are strong enough for our current detectors, we need extremely massive accelerating bodies. Black holes on it's own do not satisfy this condition. However certain binary systems do. Fig.11 shows a diagram of the known masses that were detected up until 2018. The last year there have been many more detections like binary neutron stars, binary black holes but also the first black hole and neutron star merger. This thesis is mainly focused on the merger of binary black holes.

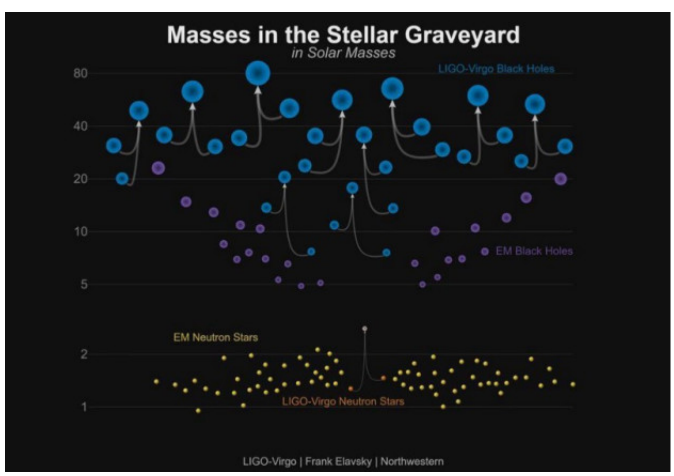

Figure 11: Known masses detected up until 2018. This diagram shows multiple sources found threw gravitational waves as well as some detections of single black holes and neutron stars found by the means of X-ray radiation. (19)

The merger of binary black holes happens in three phases. The first phase is called the *inspiral* and describes the first step in which the black holes spiral in around a shared center of mass, slowly decreasing in relative distance. During the inspiral, the system loses energy by emmiting gravitational waves. This energy loss causes the black holes to spiral inwards, decreasing in orbit. This decrease in orbital radius causes the velocity of the black holes to increase which causes more gravitational waves to be emitted. The emmiting of gravitational waves at the beginning of the inspiral is still very weak due to the great distance and slow velocities of the two black holes. While the black holes spiral closer together the signal will become stronger, making it easier to detect. Other stars accreting around the black holes might cause a loss of angular momentum. While they get closer into the inspiral the orbits will appear more circulair. The last stable orbit before it enters the next phase is called the innermost stable circulair orbit (ISCO).

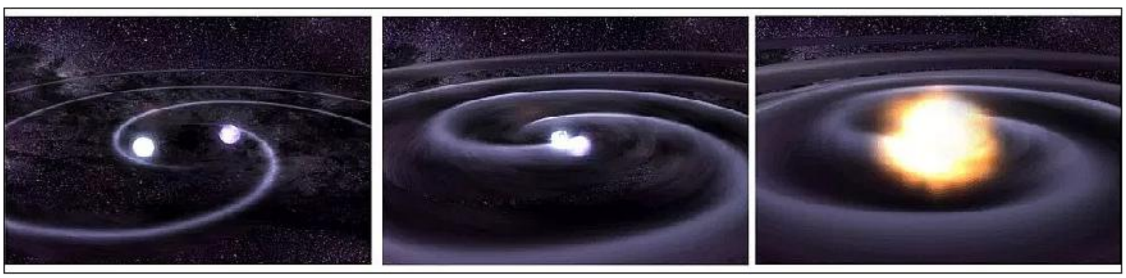

Figure 12: The three phases of merger in a binary black hole system; the inspiral, the merger and the ringdown.(20)

The next phase is the *merger*. When the two black holes come at the end of their inspiral, they merge. This is where the two smaller black holes transform into one larger black hole. The mass of the newly formed black hole is slightly smaller than the sum of the two original ones due to the energy loss of the emmited gravitational waves. The merger shows a high peak in the emmision caused by the high velocities in this phase.

The merger ends in a *ringdown* phase where the newly merged black hole finds a stable state. The distortions in shape are corrected by the emission of gravitational waves, going from an elongated spheroid shape into a perfect sphere. The final shape might slightly defer due to the spin of the black hole. (21)

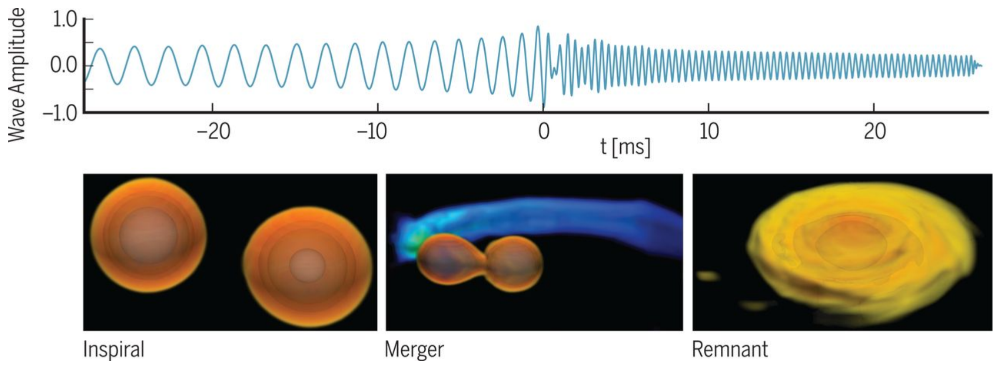

Figure 13: A gravitational wave signal from two a merging binary black hole system. Showing the three phases of merger; inspiral, merger and ringdown. (22)

Fig.13 shows the transformations for the gravitational wave signal through all three phases of merger. During the inspiral phase, the velocities are still quite low because of the relatively large distances between the two black holes. Because of these low velocities, the inspiral phase is very slow resulting in a long signal with a relatively low amplitude. In the merger phase, the distance between the black holes decreases, while the spiraling increases in velocity. The high velocities cause a stronger signal of gravitational waves. The amplitude keeps increasing until the actual merge causes a peak in the gravitational wave signal. After this peak the ringdown phase stabilizes the newly formed black hole, emmiting gravitational waves. These waves will have a much lower amplitude until they finally fade out and the merger comes to an end.

4 Data analysis of the GW signal

In this chapter we take a look at the data-analysis of a gravitational wave signal. The data used for this analysis comes from the LIGO-VIRGO open science center (9). So far the LIGO-VIRGO collaboration has made three runs of observations, where each run the detectors were improved. The first run, O1, was from 12 September 2015 to 19 January 2016, the second, O2, from 30 November 2016 until 25 August 2017 and the last run , O3, ran from 30 september 2019 till 1 November 2019. These runs have given us a lot of data for a further study in gravitational wave signals. In this chapter we mostly focus on the very first detected gravitational wave event, GW150914. This signal came from a binary black hole merger of two black holes with masses of $35.6M_{\odot}$ and $30.6M_{\odot}$. (10)

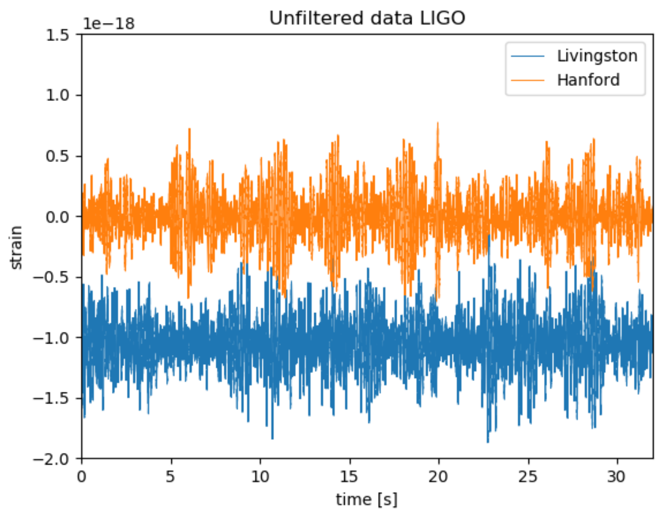

Figure 14: Imported data from Livingston and Hanford before filtering of the signal. Both strings are 32 seconds logn with a frequency of 4069 Hz.

With this analysis the two gravitational wave signals from the Livingston and Handford detector are observed and compared, using a Python based script. They are both filtered of noise with multiple filtering techniques to find the underlying signal of the binary black hole merger. At last the data is compared with a numerical template, theoretically determined with general relativity. (24)

To begin, both the data from Livingston and Handford are imported as a 32 second file in which the strain is given for a certain time. These files can both be found in the catalog of the open science center (9). Fig.14 shows the imported data of both the detectors before filtering. This datastrain does not yet reveal much information about the signal. Since the amplitude of the noise is much higher than that of our signal we are not able to see the signal in this given strain. Therefor to find the signal, multiple filtering techniques are used. (9)

Next to the data from Hanford and Livingston, there is also a theoretical template imported to compare with the data from LIGO. This template was already determined and published by LIGO (23). The template shows a typical merger signal as described in section 3.2 for two black holes of 26 $M_{\odot}$ and 29 $M_{\odot}$. The template can be seen in fig.16.

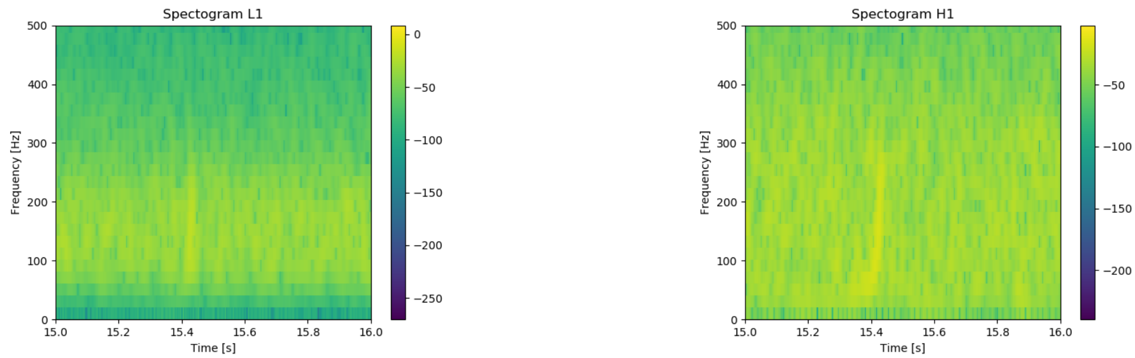

(a) Spectrogram Livingston data. (b) Spectrogram Hanford data.

Figure 15

Before we start the filtering process it can be convenient to make a spectrogram of the data. A spectrogram is a figure that shows the frequency domain over time. It also shows the power of the signal by varying in brightness. Fig.15 presents the spectrograms of the two imported datastrains. Both show a bright vertical peak around 15.4 seconds, showing an increase in power, visualizing the signal for the binary black hole merger.

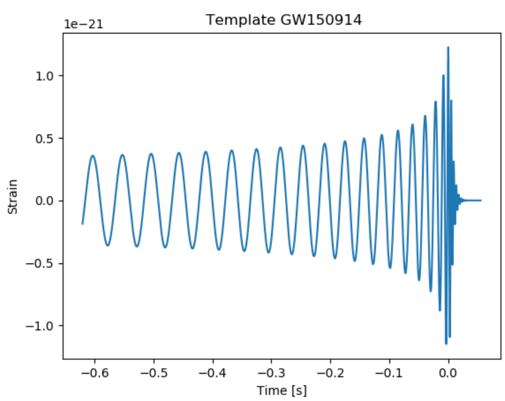

Figure 16: Numerical relativity template for a binary black hole merger for two black holes of 36 $M_{\odot}$ and 29 $M_{\odot}$.

To try and take a better look at the signal we can plot an ASD (amplitude spectral density). Even though the amplitude of the noise is much bigger than the signal itself, the signal does have more power for some frequencies. An ASD plots the power of the signal for certain frequencies giving us a better idea of the frequency content. It does this by fourier transformation of the time domain to a frequency domain,

$$E = \int_{-\infty}^{\infty} |x(t)|^2 dt, \tag{9}$$

where E is the energy of the signal $x(t)$ given as a function of time. This can be fourier transformed with Parseval's theorem:

$$\int_{-\infty}^{\infty} |x(t)|^2 dt = \int_{-\infty}^{\infty} |\hat{x}(f)|^2 df, \tag{10}$$

for which,

$$\hat{x}(f) = \int_{-\infty}^{\infty} \exp^{-2\pi i f t} x(t) dt, \tag{11}$$

is the fourier transform given in the frequency domain.

Fig.17a shows the ASD for GW150914. The figure shows multiple peaks in the amount of power of which one of these will probably be the signal. However in this situation the signal can not be seen because it is of such short time and the plot averages over 32 seconds. Another reason for this is that the signal is relatively low. The spectral lines (peaks) are caused by instrumental noise of which some can already be predicted beforehand, such as engineered noise caused by resonance (500 Hz and harmonics). There will also be some noise around 60 Hz and the harmonics. Further information about other sources of noise will be discussed later on.

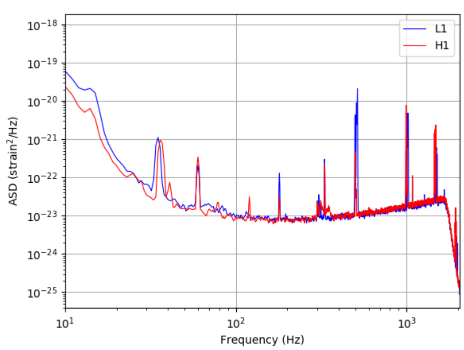

(a) The ASD of the data from Livingston and Hanford, plotting the power of the signal against the frequency.

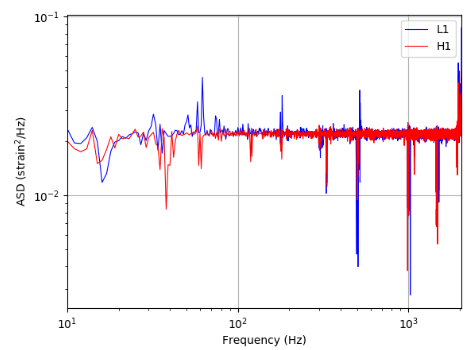

(b) The ASD of the data after whitening from Livingston and Hanford.

Figure 17

The ASD is plotted between 10 Hz and 2000 Hz. One of the reasons for this is that the frequency below 10 Hz isn't properly calibrated. Besides this, the data above 2000 Hz isn't valid because of the nyquist frequency. The nyquist frequency is the maximum frequency given at a certain sampling rate for which the signal can be fully constructed, $f_N = fs/2 = 4096/2 = 2048$ Hz.

Next a few filtering techniques are applied in order to filter out the noise. First the data is whitened with a whitening filter. A whitening filter is a way of describing the data as deviations from the mean value. This way the data can be shown as deviation from the noise. By whitening the data, the ASD will be flattened to make sure all frequencies contribute equally as shown in fig.17b.

The next step in filtering is applying a butterworth bandpass filter. This bandpass filter cuts off frequencies outside of a certain chosen bandwidth. The butterworth filter can be adjusted for different orders of the cut-off angle (fig.18). Since we know from experience that the signal will be between the frequency band of 20 Hz - 300 Hz we can bandpass for this frequency range. Fig.19 shows the signal after applying a bandpass filter for both Livingston and Hanford. The data clearly shows a large peak in the signal around 15.2 seconds. (25)

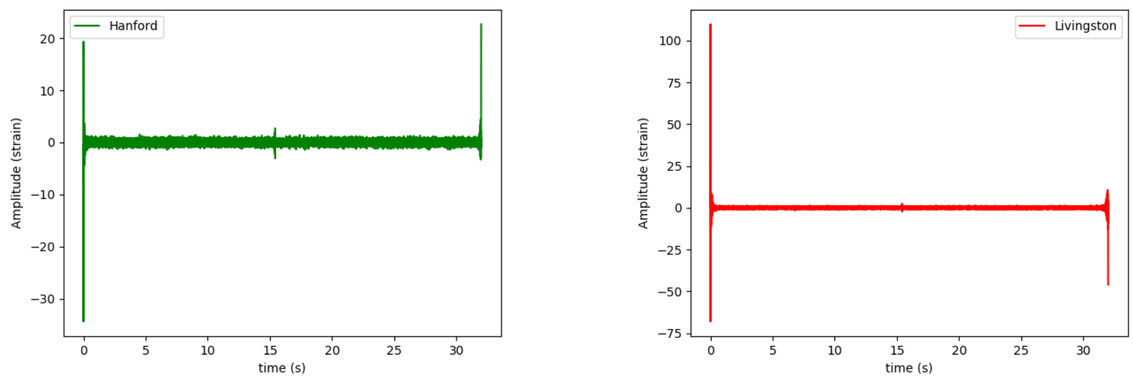

Figure 19: The data of the signal after whitening and applying a bandpass filter. With the data for Hanford on the left and the data for Livingston on the right it can be seen that for both there is a large peak in the amplitude around 15.2 seconds which shows the signal for the merger.

When zooming in on this peak it shows a clear signal of merger for two black holes (fig.20). When comparing the signal from Livingston and Hanford it can be seen that there appears to be a time shift of 7 ms. This shift is caused by the distance between the detectors which lay on the same line with the source of emission. This causes the signal to appear 7 ms earlier at the detector in Livingston than it does in Hanford.

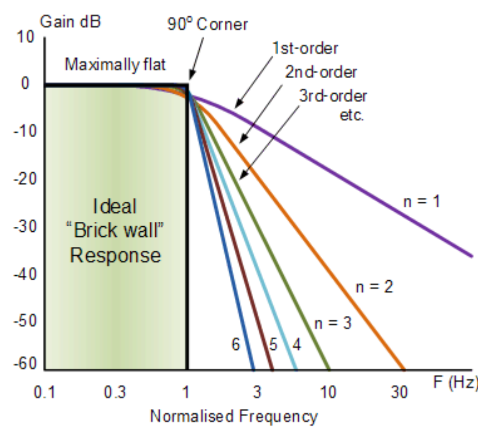

Figure 18: A butterworth bandpass filter for different orders of the cut-off angle. (25)

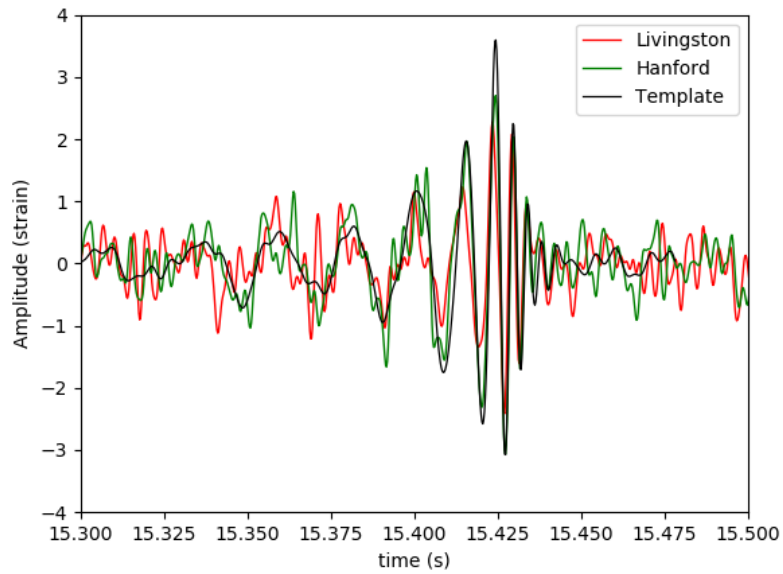

Figure 20: Gravitational wave data after whitening and bandpassing the signal from Livingston and Hanford. Both compared to a numerical relativity template.

At last there is also the option of using notch filters. A notch filter can be used to remove a precise small band of frequencies. Instead of the butterworth bandpass filter which passes all frequencies above or below a certain frequency, a notch filter rejects all frequencies for a small bandwidth. This can be used to remove the spectral lines in the signal (26). A notch filter fits in a frequency response in the form of a notch. The depth and width of the notch can be adjusted with the quality factor Q, which can be determined using $Q = (f_2 - f_1)/f_{null}$, with f_1, f_2 and f_{null} given as in fig.21.

The largest spectral lines are known to be caused by instrumental effects. The notch filters are added around the following frequencies:

- 60*n Hz (*n for the harmonics) due to electromagnetic shielding and magnetic coupling to the mirror suspensions.
- 500*n Hz thermal noise of the mirrors.
- 9 Hz and 13.8 Hz due to bounce and roll modes of the mirrors.
- 300*n Hz of vibrations in the suspension that hangs the beam splitter.

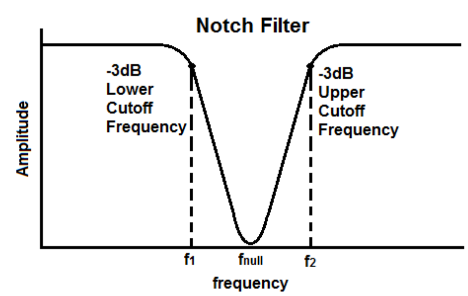

(a) The frequency response of a notch filter. (28)

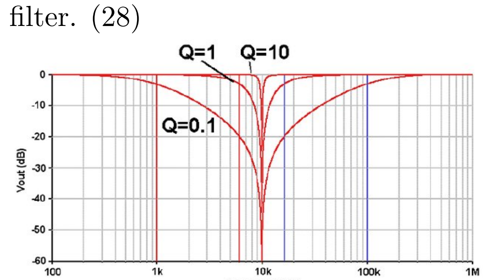

(b) A notch filter for different values of the quality factor Q. (27)

Figure 21

- calibration lines by moving the end mirrors during O1:
  - L1: 33.7, 34.7, 35.3, 331.3, 1083.1 Hz
  - H1: 35.9, 36.7, ,37.3, 331.9, 1083.7 Hz

- More spectral lines can be found at the open science center (9). This research only consideres the most obvious spectral lines mentioned above.

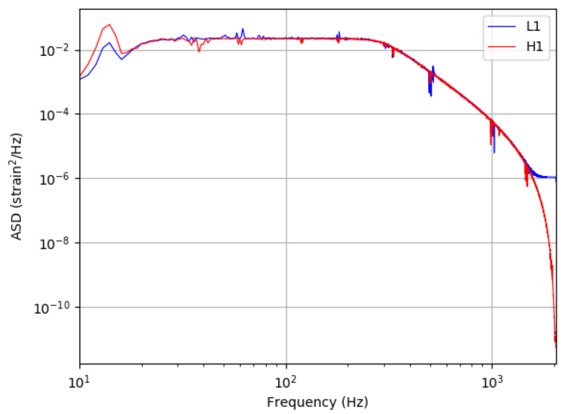

Figure 22: ASD of the data after filtering through whitening, bandpassing ans notching.

When we look at the ASD after notching it is noticeable that the ASD decreases after 300 Hz due to the bandpass filter. It is also almost entirely removed from spectral lines, comparing fig.22 after notching with fig.17b.

5 Physical aspects of a BBH merger

5.1 Newtonian mechanics

To determine a theoretical gravitational wave signal we need general relativity, but with Newtonian mechanics we can however already look at some basic properties of the black hole merger. We can start by analyzing the data based on what we know of black holes. We will derive a few Newtonian properties and check these with the data found by LIGO.

We first start by ananlyzing some black hole properties. The definition of a black hole is stated as "a region of space-time where the gravitational field is so intense that neither matter nor radiation can escape." (29). The radius for which nothing can escape a black hole is called the Schwarzschild radius,

$$r_{Schwarz}(m) = \frac{2Gm}{c^2}, \tag{12}$$

with m the mass of the object, $G = 6.6710^{-11} m^3/s^2kg$ the gravitational constant and $c = 2.99810^8 m/s$ the speed of light. Every non-spinning mass within this radius must be a black hole.

The energy that is emitted by a binary black hole system can be defined as the quadrupole moment, Q_{ij}, which can be compared to the dipole moment of electromagnetic waves. With gravitational waves there is no dipole moment. For a mass-energy density of $\rho(\vec{r})$, the gravitational monopole moment, $\int \rho(\vec{r}) d^3r$, would be the total mass-energy, which in this case is constant so there is no gravitational monopole moment. The dipole moment, $\int \rho(\vec{r})\vec{r} d^3r$, is in this case just the center of mass-energy which does not change in a center of mass frame, so there is no static dipolar gravitational radiation either. The next possible moment is the quadrupole moment which is not conserved. This means that there is a gravitational quadrupole moment, $I_{ij} = \int \rho(\vec{r}) r_i r_j d^3r$. (30)

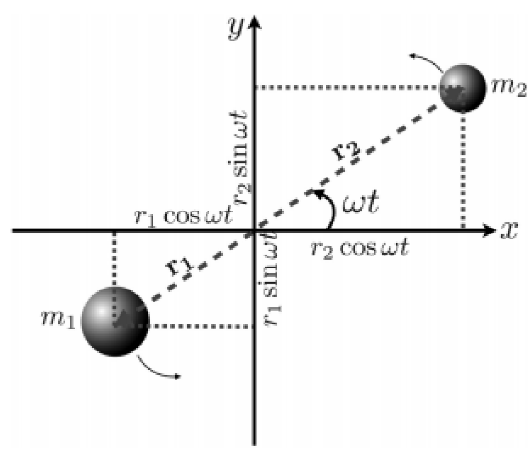

Figure 23: A two-body system with two masses orbiting the same center of mass. (31)

In a two-body system in the xy-plane with m_1 and m_2 orbiting the same center of mass we can calculate a quadrupole moment:

$$Q_{ij} = \int d^3x \rho(x)(x_i x_j - \frac{1}{3} r^2 \delta_{ij}), \tag{13}$$

with $r^2 = x^2 + y^2$, δ_{ij} is the Kronecker-delta function and $z = 0$ because of the 2 dimensional system this can be writen as,

$$Q_{ij} = \sum_{A\epsilon\{1,2\}} m_A \begin{pmatrix} \frac{2}{3}x_A^2 - y_A^2 & x_A y_A & 0 \\ x_A y_A & \frac{2}{3}y_A^2 - x_A^2 & 0 \\ 0 & 0 & -\frac{1}{3}r_A^2. \end{pmatrix} \tag{14}$$

Using $x = rcos(\omega t)$, $y = rsin(\omega t)$ and the goniometric idenitities $cos^2(\omega t) = \frac{1}{2}+\frac{1}{2}cos(2\omega t)$ and $sin^2(\omega t) = \frac{1}{2} - \frac{1}{2}cos(2\omega t)$, the above equation can be reduced to:

$$Q_{ij}^A(t) = \frac{m_A r_A^2}{2} I_{ij}, \tag{15}$$

with $I_{xx} = cos(2\omega t) + \frac{1}{3}$, $I_{xy} = I_{yx} = sin(2\omega t)$, $I_{yy} = \frac{1}{3} - cos(2\omega t)$ and $I_{zz} = -\frac{2}{3}$. This gives a total quadrupole moment of $Q_{ij} = \frac{1}{2}\mu r^2 I_{ij}$.

The quadrupole moment can give us information about the rate at which the energy is emitted in gravitational waves. For a certain distance from the source d_L, the strain can be expressed in teh quadrupole moment Q_{ij}:

$$h_{ij} = \frac{2G}{c^4 d_L}\frac{d^2Q_{ij}}{dt^2}. \tag{16}$$

The energy rate over time is equal to the flux for a sphere of radius d_L,

$$\frac{dE_{GW}}{dt} = -F_{GW} = \frac{c^3}{16\pi G}\iint |\dot{h}|^2 dS = \frac{1}{5}\frac{G}{c^5}\sum_3 {}_{i,j=1}\frac{d^3Q_{ij}}{dt^3}\frac{d^3Q_{ij}}{dt^3}. \tag{17}$$

Taking the third time derivative of the quadrupole moment we find:

$$\frac{d^3Q_{ij}}{dt^3} = 4\omega^3\mu r^2 \begin{pmatrix} \sin(2\omega t) & -cos(2\omega t) & 0 \\ -cos(2\omega t) & -sin(2\omega t) & 0 \\ 0 & 0 & 0 \end{pmatrix}. \tag{18}$$

Substituting this in eq. 17 gives a value for the radiated power:

$$\frac{dE_{GW}}{dt} = \frac{32}{5}\frac{G}{c^5}\mu^2 r^4 \omega^6. \tag{19}$$

The power radiated in the form of gravitational waves is equal to the loss of orbital energy. This means we can state, $\frac{dE_{orb}}{dt} = -\frac{dE_{GW}}{dt}$. For an orbital energyloss of $dE_{orb} = \frac{G(m_1+m_2)\mu}{2r}$ we can now equate the two by using Kepler's third law ($r^3 = GM/\omega^2$), finding:

$$\frac{(m_1 m_2)^{3/5}}{(m_1+m_2)^{1/5}} = \frac{c^3}{G}(\frac{32}{15}\omega^{-11/3}\frac{d\omega}{dt})^{3/5} \tag{20}$$

Integrating this will give a relation of the chirp mass as a function of the frequency:

$$\frac{1}{f_1^{8/3}} - \frac{1}{f_1^{8/3}} = \frac{256}{5}\pi^{8/3}\frac{G^{5/3}M_{schirp}^{5/3}}{c^{5/3}}(t_2 - t_1) \tag{21}$$

The equality on the left side of eq. 20 now gives the definition of the chirp mass. The chirp mass is a mass scale often used when working with binary merges. Since the chirp mass is just a mass scale it is not possible to determine the individual masses of the binaries. However a rough estimation can be made with the following method. It is possible to find a value of the highest frequency and use this to approximate a value for the individual masses. We know that when the two black holes start to coalesce, their seperation will be equal to the sum of their Schwarzschild radius (equation 12), for which we can state:

$$r_1 + r_2 = \frac{2G}{c^2}(m_1 + m_2) \tag{22}$$

If we know use Kepler's third law,

$$\omega^2 = \frac{G(m_1 + m_2)}{(r_1 + r_2)^3}, \tag{23}$$

we can find the angular frequency given at the start of coalescense. Since this is the begin of the merger phase, we can assume that the angular frequency will reach it's maximum around this point in the signal. This gives us an angular frequency of,

$$\omega_c = f_c \pi = \frac{1}{\sqrt{8}} \frac{c^3}{G(m_1 + m_2)}. \tag{24}$$

As been shown in fig. 15 we can convert the signal into a frequency-time plot showing us an average (of Livingston and Hanford) maximum frequency of around $f_c = 320Hz$. This would give a total mass of 71 $M_\odot$. Now that we have the total mass we can use eq. 21 to estimate the chirp mass and determine the masses of the individual black holes. Using the same frequency-time plot as before we can observe values for $f_1 = 50Hz$, $f_2 = 300Hz$, $(t_2 - t_1) = 0.07$ s. Plugging this in to the equation for the chirp mass we find a value of $M_{chirp} = 29\ M_\odot$. With a value for the chirp- and total mass of the system we can derive the individual values for the masses. Defining $m_1 = \alpha M$ and $m_2 = (1 - \alpha)M$ and substituting this in the equation for the chirp mass:

$$M_{chirp} = \frac{(\alpha(1-\alpha)M^2)^{3/5}}{M^{1/5}} = (\alpha(1-\alpha))^{3/5} M. \tag{25}$$

Inserting the values for the chirp- and total mass followed by the abc-formula we find $\alpha = 0.55$. Giving individual masses of $m_1 = 39.1M_\odot$ and $m_2 = 31.9M_\odot$. Comparing this to the actual data published by LIGO which yields $M = 65M_\odot$, $M_{chirp} = 30M_\odot$, $m_1 = 29M_\odot$ and $m_2 = 36M_\odot$, these values are in reasonable agreement keeping in mind that the data was roughly estimated from a figure.

It is also possible to make an estimation of the total energy radiated. If we again assume that the final point of merger is the sum of the Schwarzschild radii, we can insert eq.12 in the formula for the radiated power (eq.19). While LIGO determined the power radiated to be equal to $3M_\odot$, the estimation gives a value of $4M_\odot$, which is still fairly in agreement. (31)(32)

5.2 General relativity

Even though some assumptions of a black hole binary system can be made only using Newtonian mechanic, general relativity plays the main role in extremely massive and accelerating bodies. This chapter will review a brief explanation of general relativity and how it can be used to determine certain aspects of black hole binary systems.

The theory of general relativity is based on two main ideas. The first idea is called the Principle of equivalence. It states that an observer in space, accelerating with an acceleration of g can not know the difference from standing on an inertial mass being subject to a gravitational force with the same value for g. The second idea is that massive accelerating bodies bend light. The more massive the body, the more extreme the light is bend. The theory describes how space exists of four dimensions, being three dimensions of space and one dimension of time. Keeping in mind, the postulates mentioned above, Einstein came up with the theory of gravity, in which gravity is not just a force of attraction between bodies, but where gravity is defined as the curving of space-time.

With his theory of general relativity, Einstein found a way of describing the geometry of curved space-time and called it The Einstein field equations,

$$R_{\mu\nu} - \frac{1}{2}g_{\mu\nu}R + g_{\mu\nu}\Lambda = \frac{8\pi G}{c^4}T_{\mu\nu}, \tag{26}$$

with G the gravitational constant and c the speed of light, also known as $G_{\mu\nu} = 8\pi G T_{\mu\nu}$. The Einstein field equations contain a lot of other constants and so called tensors. In the following part the Einstein field equations will be further explained, defining the meaning and symbols of the equations.

As earlier mentioned, the Einstein field equations (EFEs) describe the curvature of space-time. It is often said that the equations are a way of showing two important things; They mention how mass tells space-time how to curve and show how curved space-time tells mass how to move. To get more insight on what the equations actualy present, we start by analyzing the physical meaning of the left- and right-hand side of eq. 26. The left-hand side of the equation shows the curvature of space-time, while the right hand-side of the equation describes the mass and energy of the system. When we take an even closer look, the EFEs are actually defined as 16 separate equations. The $\mu\nu$ subscript in the equations suggest a total of 4×4 equations, where μ and ν can both take on the form of the 4 dimensions of space-time, given $\mu\nu \in \{0, 1, 2, 3\}$. Where $\mu = \nu = 0$ describes the dimension of time and $\mu = \nu = 1, 2, 3$ describe the three dimensions of space. Since 6 of the equations are duplicates the EFEs consist of 10 different equations.

To give a good explanation of the EFEs we are going to derive some main concepts of space-time concerning the relativity postulates. Deriving these concepts will reveal the further meaning of the Einstein field equations. (33)

Before we can analyze the curvature of space-time, we first need to define space-time itself. Space-time can be seen as a field containing four dimensions. This field can be defined as an area (xy-plane) containing wripples (z-axis), adding a fourth dimension of time. To describe a field we can use the gradient defining the rate of change for all four dimensions in spacetime:

$$d\phi = \frac{\partial \phi}{\partial x_1}dx_1 + \frac{\partial \phi}{\partial x_2}dx_2 + \frac{\partial \phi}{\partial x_3}dx_3 + \frac{\partial \phi}{\partial x_4}dx_4. \tag{27}$$

For n dimensions this can be simplified to,

$$d\phi = \sum_n \frac{\partial d\phi}{\partial x_n}dx_n. \tag{28}$$

Now that we've defined space-time we need to include the conditions of general relativity. An important postulate is that the equations must be independent of reference frame (fig.24). If we define two reference frames x and y, we can ask ourselves if the derivatives for the reference frame x, $\frac{\partial \phi}{\partial x_n}$, is equal to the derivatives in the reference frame of y, $\frac{\partial \phi}{\partial y^n}$. To switch between reference frames we can use the chain rule to find:

$$\frac{\partial \phi}{\partial y_1} = \frac{\partial \phi}{\partial x_1}\frac{\partial x_1}{\partial y_1} + \frac{\partial \phi}{\partial x_2}\frac{\partial x_2}{\partial y_2} \tag{29}$$

A more general way of defining this is for the reference frames n and m,

$$\frac{\partial \phi}{\partial y_n} = \sum_m \frac{\partial \phi}{\partial x_m}\frac{\partial x_m}{\partial y_n}. \tag{30}$$

The above equation is meant to work on vectors. However the EFEs work with something called tensors. Tensors contain the data of multiple vectors, having N dimensions. A vector is a tensor of rank 1. When adjusting eq. 29 for the case of a tensor we find:

$$V_y^n = \sum_m \frac{\partial y_n}{\partial x_m}V_x^m, \tag{31}$$

where x and y are reference frames and n is the dimension of the tensor, V.

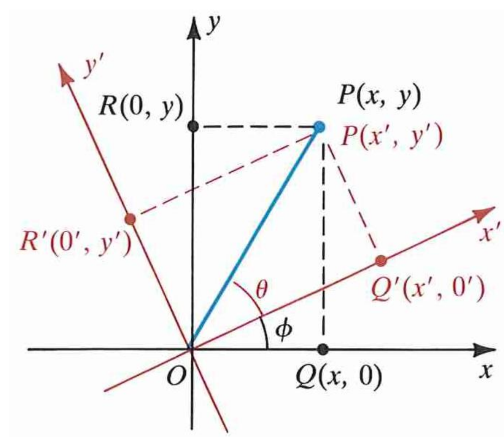

Figure 24: The same point in space observed from a different reference frame. (34)

Tensors can be stated in two different forms; the contravariant and covariant form. The contravariant form is defined as:

$$T^{mn} = A^m B^n. \tag{32}$$

If m and n can be either 1 or 2, the tensor has a total of 4 values. Substituting this definition in eq. 31 we find,

$$T_y^{mn} = \sum_{r,s} \frac{\partial y_m}{\partial x_r}\frac{\partial y_n}{\partial x_s}A_x^r B_x^s, \tag{33}$$

for which we define a new tensor $A^r_x B^s_x$ in a reference frame x having the dimensions of r and s. The most common way of using the tensor definition is the covariant way which we will be working with from now on:

$$T_{mn}(y) = \sum_{r,s} \frac{\partial x_r}{\partial y_m} \frac{\partial x_s}{\partial y_n} T_{rs}(x). \tag{34}$$

If we now apply our knowledge of tensors to the geometry of space we can define the space-time metric. We start by using the simple Pythagoras theorem to define a small space ds, $ds^2 = dx^2 + dy^2$, which can be more generalized to $ds^2 = \sum_{m,n} dx_m dx_n \delta$. Since we take ds to be so small it can be taken to be straight, for a curved space s. Using again eq. 29 we can define $dx_m = \frac{\partial x_m}{y_r} dy_r$, which we substitute in eq.34 to obtain,

$$T_{mn}(y) = \sum_{r,s} \frac{\partial x_r}{\partial y_m} \frac{\partial x_s}{\partial y_n} \frac{\partial V_r(x)}{\partial x_s}. \tag{35}$$

Substituting this is the Pythagoras theorem we find,

$$ds^2 = \delta_{mn} \sum \frac{\partial x_m}{\partial y_r} \frac{\partial x_n}{\partial y_s} dy_r dy_s, \tag{36}$$

defining the geometry of space-time and also the first unknown of the Einstein equations called the *metric tensor* g_{mn},

$$g_{mn} = \delta_{mn} \sum \frac{\partial x_m}{\partial y_r} \frac{\partial x_n}{\partial y_s}. \tag{37}$$

The metric tensor makes corrections to the Pythagoras theorem, turning flat space into curved space.

Next we will discuss the Christoffel symbol, Γ. This symbol doesn't directly occur in the EFEs, but does appear indirectly in the Ricci tensor, $R_{\mu\nu}$, which will be derived next. Since we know from Einstein's postulates that our calculations should be the same in every reference frame, we should ask ourselves if this is also true for the derivatives. Unfortunately this is not the case. The Christoffel symbol is a compensation for the change in derivative for different reference frames, $T_{mn}(x) = \frac{\partial V_m(x)}{\partial x_n}, T_{mn}(y) = \frac{\partial V_m(y)}{\partial y_n}$, for a vector V. Using eq. 34 and redefining the equation gives,

$$T_{mn}(y) = \frac{\partial x_r}{\partial y_m} \frac{\partial x_s}{\partial y_n} \frac{\partial V_r(x)}{\partial x_s} = \frac{\partial x_r}{\partial y_m} \frac{\partial V_r(x)}{\partial y_n}, \tag{38}$$

where the last part shows an inverse chaine rule, explaining for the second equation. Now defining the derivative for a different frame of reference, using eq. 31 and the product rule,

$$\frac{\partial V_m(y)}{\partial y_n} = \frac{\partial}{\partial y_n}(\frac{\partial x_r}{\partial y_m} V_r(x)) = \frac{\partial x_r}{\partial y_m} \frac{\partial V_r(x)}{\partial y_n} + \frac{\partial x_r}{\partial y_m} \frac{\partial}{\partial y_n} V_r(x). \tag{39}$$

Comparing eq. 38 and eq. 39 we find that the derivative in the y frame of reference has an extra term, which is the Christoffel symbol. This means that we can not simply use a normal derivative when we're talking about general relativity. Which is why in general relativity we talk about a special covariant derivative, ∇ defined as above:

$$T_{mn}(y) = \nabla_n V_m = \frac{\partial V_m}{\partial y_n} + \Gamma^r_{nm} V_r(x). \tag{40}$$

Taking the derivative of a tensor we derive:

$$\nabla_p T_{mn} = \frac{\partial T_{mn}}{\partial y_p} + \Gamma^r_{pm} T_{rn} + \Gamma^r_{pn} T_{mr}. \tag{41}$$

Knowing that the covariant derivative of a flat space time geometry must be zero, we can find a value for the Christoffel symbol. Applying eq. 41 for flat spacetime:

$$\nabla_p g_{mn} = \frac{\partial g_{mn}}{\partial y_p} + \Gamma^r_{pm} g_{rn} + \Gamma^r_{pn} g_{mr} = 0. \tag{42}$$

When Einstein passed this equality on to a mathematician which found that the Christoffel symbol should be equal to,

$$\Gamma^a_b c(x) = \frac{1}{2} g^{ad} \left(\frac{\partial g_{dc}}{\partial x_b} + \frac{\partial g_{ab}}{\partial x_c} + \frac{\partial g_{bc}}{\partial x_d}\right). \tag{43}$$

Now that we found the Christoffel symbol, we can determine the Ricci tensor. The Ricci tensor expresses in what measure space differs from normal Euclidean space. To express this problem we can move a vector with a certian magnitude and angle parallel along a sphere. If we place the vector on the top of the sphere going down, turning 90 degrees on the equator and up again to the starting point, the vector will not be in the same direction as the starting position. This is a result of the curvature of the sphere. To measure this difference we can derive the commutator $[\nabla_m, \nabla_n]$. Applying the commutator to a vector V, using the definition for the covariant derivative (eq. 41),

$$\begin{aligned}[\nabla_m, \nabla_n]V = \nabla_m \nabla_n V - \nabla_n \nabla_m V = (\partial_m + \Gamma_m)(\partial_n + \Gamma_n)V - (\partial_n + \Gamma_n)(\partial_m + \Gamma_m)V = \\ -([\partial_n, \Gamma_m] + [\partial_m, \Gamma_n] + [\Gamma_m, \Gamma_n])V,\end{aligned} \tag{44}$$

we have derived the Ricci tensor, $R_{\mu\nu}$. Another unknown in the EFEs is the Ricci curvature scalar, R. This scalar describes how much the volume of a geodesic ball deviates from a ball in Euclidean space and can be determined from the Ricci tensor.

At last we will derive the right-hand side of the equation, The stress energy momentum tensor, $T_{\mu\nu}$. A geodesic is the shortest distance between two points. The distance between two points can be defined as $\frac{dx_\mu}{\tau}$, with dx_μ the distance and $d\tau$ the proper time which is the time that is the same in every reference frame. To determine the shortest distance between two points, we can now minimise the distance by taking the first derivative and setting it equal to zero:

$$\nabla \frac{dx_\mu}{d\tau} = \frac{\partial}{\partial \tau} \frac{\partial x_\mu}{\partial \tau} + \Gamma = 0, \tag{45}$$

or in a different form $\frac{\partial^2 x_\mu}{\partial \tau^2} = -\Gamma$. We could describe this equality as the acceleration being equal to the Christoffel symbol. As we know from Newton's first law, the acceleration should be linearly equivalent to the force, $a = F/m$. If we combine relativity with Newton, we can assume that the Christoffel symbol should be similar to the force. More specific, the gravitational force tells us that $F = -mg$, for a potential $\phi = mgx$, keeping in mind that $F = -d\phi$. For a low gravity field and low velocity, we know that the EFEs should reduce to a Newtonian situation. These conditions given, we should be able to determine the Christoffel symbol. Since we consider a flat space-time, the metric tensor should reduce to $g = 1$, with its space derivatives small enough to neglect. This should leave us with the Christoffel symbol,

$$\frac{1}{2}\frac{\partial g_{00}}{dx} = F = -\frac{\partial \phi}{\partial x}. \tag{46}$$

Integrating both sides with respect to x, we find $g_{00} = 2\phi + constant$. Looking at it from a Newtonian point of view we can integrate Newton's gravitational force,

$$\int F \cdot dA = -\int \frac{GM}{r^2} dA = -4\pi GM. \tag{47}$$

Rewriting $M = \int \rho dV$ and using the divergence theorem we obtain,

$$-4\pi G \int \rho dV = \int \nabla \cdot F dV, \tag{48}$$

from which we can state $\nabla F = -a\pi G\rho$ or otherwise $\nabla^2 \phi = 4\pi G\rho$. Substituting eq. 46 for the potential, this results in something very similar to the Einstein field equations,

$$\nabla^2 g_{00} = 8\pi G\rho \tag{49}$$

however, this is not yet a tensor equation. Transforming the found equality in a tensor equation we find the Einstein field equations, $G_{\mu\nu} = 8\pi G T_{\mu\nu}$, with on the right-hand side the stress energy momentum tensor which is defined as the energy per unit volume or force per unit surface ($E/V = F/A$). The tensor can be expressed as a 4×4 matrix containing the four-dimensions,

$$T_{\mu\nu} = \begin{pmatrix} T_{00} & \dots & \dots & T_{00} \\ \vdots & \ddots & & \\ \vdots & & \ddots & \\ T_{03} & & & T_{33} \end{pmatrix} \tag{50}$$

To expand the equation we can look at the energy conservation within the system. Since we know that the energy is conserved we can set the derivative of the energy tensor equal to zero. However this means that the derivative of the Ricci tensor should also be zero, even though this is not the case. Deriving $\nabla R_{\mu\nu}$ and subtracting this value from the left hand-side of the EFEs we find that both sides are equal to zero. The EFEs now state:

$$R_{\mu\nu} - \frac{1}{2} g_{\mu\nu} R = \frac{8\pi G}{c^4} T_{\mu\nu}, \tag{51}$$

where c^4 is of dimensional purposes. The last term of the EFEs, $g_{\mu\nu}\Lambda$ is a very small term for which it is often left out of the equations. This term balances the effects of gravity in the universe, representing a counter force, successfully deriving the Einstein field equations.

6 Discussion and conclusion

In this thesis we analyzed the gravitational wave signal from the binary black hole merger GW150914. We did this by performing a data-analysis on the gravitational wave signal from LIGO observatories. We compared the datastrains from the two LIGO detectors build in Livingston and Hanford. Observing that noise plays a large part in gravitational wave detectors, we developed a script which filters the datastrains from noise using several filtering techniques. First the signal was whitened to flatten the ASD. Knowing in which frequency-band the merger signal would appear, we next applied a butterworth bandpass filter for a frequencyband of 20 Hz to 300 Hz. Finally, we applied a notchfilter to reject certain spectral lines which are caused by instrumental noise. After applying filtering we obtained a signal matching the theoretical waveform of a binary black hole merger. Also comparing both the datastrains with a general relativity template, the signal seemed to be in perfect agreement.

After finding the gravitational wave signal we applied a theoretical analysis to test our findings. We found that the gravitational wave signal of a binary black hole merger includes mostly general relativity caused by the extreme masses and high velocities of the system. This thesis did not mainly focus on general relativity due to a minimum amount of time. However the Einstein field equations were briefly mentioned, showing how mass tells space-time how to curve and explaining how curved space-time shows mass how to move. Not being able to apply general relativity on the signal, we did however perform a rough estimation using Newtonian mechanics. Deriving multiple properties for black holes and binary systems, we made an estimation of the masses and radiated energy. Obtaining values for the individual masses of $39.1M_\odot$ and $31.9M$ and a radiated energy of $4M_\odot$, this was roughly in agreement with the values published by LIGO ($m_1 = 29M_\odot, m_2 = 36M_\odot, E_{rad} = 3M_\odot$).

In future research a more specific analysis on general relativity could be applied to the data, checking with the data published from LIGO or other gravitational wave detectors. Since the network of detectors keeps expanding, a more specific analysis could be done in the future. Being able to detect the same event on a more extended network would result in better comparisment between data. This could lead to a higher reliability and a more advanced sky localization system. With the future plans for the Einstein telescope on earth and the LISA project in space we have a bright future to look forward to. The Einstein telescope will be even more sensitive, with a much wider frequency-band, predicted to find new events several times a day. This gives us the opportunity of discovering different parts of the universe in a much faster rate than is possible today. The LISA will be even more remarkable, especially focusing on an entirely different frequencyband than the detectors present on earth. The LISA project will open our eyes about an entire new spectrum of the universe, maybe even finding new sources of gravitational wave events.

References

[1] SXS,
url = ”https://www.black-holes.org/”

[2] Science alert,
url = ”https://www.sciencealert.com/gravitational-waves”

[3] Wikipedia Gravitational wave events,
url = ”https://en.wikipedia.org/wiki/Gravitational_waveHistory”

[4] Nicholas Arnaud, ”Gravitational waves: a taxonomy”, 10/2017

[5] ”Gravity: An introduction to Einstein’s General Relativity”, James Hartle, first edition 2014

[6] Alexandre Le Tiec and Jerome Novak, ”Theory of gravitational waves”, 07/2016

[7] Markus Pössel, ”Sources of Gravitational Waves: The Most Violent Events in the Universe”, Universe today, 02/2016

[8] Wikipedia Interferometers
url = ”https://en.wikipedia.org/wiki/Gravitational-wave_observatory#/media/File:LIGO_schematic_(multilang).svg”

[9] Gravitational wave open science center
url = ”https://www.gw-openscience.org/static/workshop2/course.html”

[10] LIGO Caltech,
url = ”https://www.ligo.caltech.edu/page/learn-more”

[11] EGO,
url = ”http://www.ego-gw.it/public/virgo/virgo.aspx”

[12] Christopher Berry, ”Dirichlet Process Gaussian-mixture model: An application to localizing coalescing binary neutron stars with gravitational-wave observations”, 08/2019

[13] VIRGO,
url = ”http://www.virgo-gw.eu/”

[14] Einstein telescope,
url = ”https://www.einsteintelescope.nl/”

[15] LISA,
url = ”https://www.lisamission.org/”

[16] GEO600,
url = ”https://www.geo600.org/1744858/news_publication_10587920”

[17] Chandra X-Ray Observatory,
url = "https://chandra.harvard.edu/photo/2019/black_hole/"

[18] Nola Taylor Redd, "What are black holes?", 07/2019

[19] Sciencesprings,
url = "https://sciencesprings.wordpress.com/2019/03/30/from-ethan-siegel-ask-ethan-why-havent-we-found-gravitational-waves-in-our-own-galaxy/638b5-0rmxatid4ji0szce3/"

[20] EO Portal directory,
url = "https://directory.eoportal.org/web/eoportal/satellite-missions/v-w-x-y-z/virgo-interferometer"

[21] Wikipedia Binary black hole mergers,
url = "https://en.wikipedia.org/wiki/Binary_black_hole"

[22] Bernd Brgmann et Al, "Fundamentals of numerical relativity for gravitational wave sources", 07/2018

[23] Template .txt file,
url = "https://losc.ligo.org/s/events/GW150914/GW150914_4_NR_waveform.txt"

[24] Data-ananlysis GW open-science center,
url = "https://www.gw-openscience.org/s/events/GW150914/GW150914_tutorial.html"

[25] Electronics tutorials,
url = "https://www.electronics-tutorials.ws/filter/filter_8.html"

[26] George Ellis, "Filters in control systems", 2012

[27] "Modelling of an Optical Coherent QPSK Transmission System PART-II", Arunprasanth Sakthivel, 08/2010

[28] Learning about electronics,
url = "http://www.learningaboutelectronics.com/Articles/Quality-factor-calculator.php"

[29] Lexico dictionary,
url = "https://www.lexico.com/definition/black_hole"

[30] "Overview of gravitational radiation',
url = "https://www.astro.umd.edu/$\sim$ $miller/teaching/astr498/lecture24.pdf$"

[31] "The basic physics of the binary black hole merger GW150914", LIGO Scientific and VIRGO Collaborations, 10/2016

[32] "An analysis of the LIGO discovery based on Introductory Physics", Harsh Mathur, 01/2018

[33] "Einstein field equation for beginners",
url = "https://www.youtube.com/watch?v=foRPKAKZWx8"

[34] bymath,
url = "http://www.bymath.com/studyguide/angeo/sec/angeo1.htm"

7 Appendix

The Python based script used for the filtering process in chapter 4 can be found under the following link: "https://github.com/suzannelexmond/filtering_process_GW150914.git"